IOSR Journal of Mechanical and Civil Engineering (IOSR-JMCE)
e-ISSN: 2278-1684,p-ISSN: 2320-334X, Volume 18, Issue 4 Ser. III (Jul. – Aug. 2021), PP 13-28
www.iosrjournals.org

Numerical Investigation of Shear Behavior of RC T-beams Strengthened by Ultra High-Performance Fiber Reinforced Concrete (UHPFRC)

Ghada M. Hekal[1,3], Magdy I. Salama[2], Galal Elsamak[2], Ahmed H. Almaadawy[2]
[1]*Department of Civil Engineering, Faculty of Engineering, Menoufia University, Egypt.*
[2]*Department of Civil Engineering, Faculty of Engineering, Kafrelsheikh University, Egypt.*
[3]*Higher institute of Engineering and Technology, Menoufia, Egypt.*

Abstract
This paper proposes numerically different strengthening techniques for reinforced concrete (RC) T-beams based on finite element analysis (FEA), in which ultra high performance fiber reinforced concrete (UHPFRC) plates are affixed to RC T-beam using epoxy adhesive to improve the shear capacity. Three different experimental works of literature were used to validate the beam numerical models. Beams were modelled using 2D shell element model to reduce the central processing unit (CPU) time and one half of beam was simulated to take the advantage of symmetry. The strengthening techniques included, two-sided strengthening, one-sided strengthening, vertical strips, and U-shaped strengthening technique. The FEA results showed that the two-sided strengthening increased the ultimate load, stiffness, and ductility and changed the failure pattern from shear to flexural. However, the one-sided strengthening provides an increase in ultimate load close to two-sided strengthening but could not be able to change the failure pattern of the control beam. U-shaped strengthening was the best technique as it gave the maximum load compared to other strengthening cases in addition to a better increase in stiffness and ductility.

Keywords: *ABAQUS; UHPFRC; 2D shell element; Plasticity; RC; FEA; Debonding; CPU.*

Date of Submission: 22-07-2021 Date of Acceptance: 07-08-2021

I. Introduction

In the last two decades, different techniques of strengthening RC structures have been developed, such as using fiber reinforced polymer (FRP), concrete and steel jacketing, shotcrete, ultra high-performance fiber reinforced concrete (UHPFRC) and the addition of structural element. The addition of structural elements is a reliable method for strengthening which can increase the strength, the stiffness or the ductility of the structure but also presents significant disadvantages so the advantages and disadvantages of each strengthening technique should be considered to determine the best appropriate technique for each situation. Strengthening using UHPFRC is one of the best techniques that has proven its efficiency in strengthening operations, due to the superior properties that this material possesses in tension and compression as well as its resistance to rust and ease of implementation. Many studies have dealt with the mechanical properties of this material, for example [1-5].

Lampropoulos et al. [6] experimentally studied the efficiency of the use of UHPFRC layers for the strengthening of existing RC beams. Three beams strengthened with 50 mm layer in the tensile side (ST_UHPFR_TS), 50 mm in the compressive side (ST_UHPFR_CS), and three-side jacket with 50 mm thickness (ST_UHPFR_3SJ) in addition to the reference beam. The study concluded that in case of specimens strengthened with UHPFRC in the compressive side, increment of the tensile strength of UHPFRC was not considerably affecting the response of the strengthened specimens. In case of strengthened specimens with UHPFRC in the tensile side, the ultimate moment was increased when UHPFRC tensile strength was increased. The respective increment for strengthened specimens with three side jackets (ST_UHPFRC_3SJ) was significantly higher compared to others.

Habel et al [7] investigated the flexural performance of composite concrete-UHPFRC elements. Three configurations for the optimum performance of the composite's elements were proposed. In the first configuration, the researchers proposed that for the protection of the concrete layer a thin UHPFRC layer, of at least 30 mm, should be cast on the existing RC member. In the second configuration, steel bars can be added to the UHPFRC layer to replace the deteriorated bars of the RC member, in this case the layer should have a depth of at least 50 mm. Finally, the aim of the third configuration was to increase the strength of the existing members. Therefore, it was suggested that

*Corresponding author, Teaching Assistant., E–mail address: ahmed_almaadawy@eng.kfs.edu.eg.

steel bars should be added to the UHPFRC layer. They concluded that, additional reinforcement in the UHPFRC layer is the most efficient way to increase the bending resistance.

Panigrahi et al. [8] investigated experimentally the strengthening of shear deficient RC T-beams with externally bonded GFRP sheets. All beams were tested under four-point bending. Different strengthening configurations using GFRP layers were studied such as, inclined strips, U-shaped strips, webs opening and sides plates at shear span only. Test parameters included GFRP amount and distribution, bonded surface, number of layers and fiber direction. The GFRP layers were affixed to the concrete surface using mechanically anchored bonded. The experimental results of tested beams with and without openings showed that this method eliminates the debonding and utilizes the GFRP sheets to its fullest capacity, thus increasing the shear capacity considerably.

Zhang et al. [9] explored experimentally the flexural behavior of RC beams strengthened by toughness-improved ultra high-performance concrete (UHPC) layer. The results showed that the cracking and flexural resistance of the strengthened beams with the UHPC layer toughened by the placement of steel wire mesh, oriented steel fibers and moderate-temperature steam curing were further improved. The most evident improvement in cracking and flexural resistance was observed in the strengthened beam with the addition of steel wire mesh.

Al-Osta et al. [10] investigated, the effectiveness and efficiency of two different techniques for strengthening of RC beams using UHPFRC i.e.; (i) by sand blasting RC beams surfaces and casting UHPFRC in-situ around the beams inside a mold and (ii) by bonding prefabricated UHPFRC strips to the RC beams using epoxy adhesive. Beams under each technique were strengthened in three different strengthening configurations; (i) bottom side strengthening (ii) two longitudinal sides strengthening (iii) three sides strengthening. The results showed that the strengthened beams on three sides showed the highest capacity enhancement, while beams strengthened only at the bottom side showed the least enhancement. Additionally, finite element (FE) and analytical models were developed to predict the behavior of the beam specimens. The result of the models showed good agreement with experimental results, as they were able to predict the behavior of the beams with high accuracy.

Bahraq et al. [11] studied experimentally and numerically the shear behavior of RC beams strengthened with UHPC jackets using two sides and three sides jackets. The shear span to depth ratio was one of the parameters (a/d = 1; 1.5 and 2), which was studied in addition to the strengthening configuration. The retrofitted beams with three-sided jacketing and lower a/d ratio showed a higher failure load. However, the enhancement of the load carrying capacity, as compared to that of control beams, was significantly lower at the a/d ratio of 2.0 as compared to that at the a/d ratios of 1.0 and 1.5. While failure of control beams took place in shear, the failure of two-sided strengthened beams shifted to flexure-shear mode and to the flexure mode for the three-sided strengthened beams. No debonding failure was observed in the experimental work. Moreover, the debonding failure was not observed in some experimental tests [12-17].

Sakr et al. [18] studied experimentally and numerically the shear behavior of RC beams strengthened with UHPFRC plates. Strengthening the RC beams was based on the use of two different techniques: (a) one longitudinal side strengthening (b) two longitudinal sides strengthening. Moreover, strengthening RC beams with reinforced or non-reinforced prefabricated UHPFRC plates was also investigated. The experimental results showed that the UHPFRC plates increased the ultimate load carrying capacity and ductility, compared with the control beam, which failed in shear. A point to be noted is that the UHPFRC plates were bonded to the surface of concrete using epoxy adhesive, and that the failure was debonding in the one-sided strengthened beam. Steel connectors were used to the one-sided strengthened beam which led to increase both of load carrying capacity and the bond between concrete surface and UHPFRC plates. Consequently, debonding failure mode was prevented.

The current study investigated numerically the shear behavior of RC T-beams strengthened with UHPFRC plates. Three literature experimental studies were used to validate the beam numerical model. Then, a parametric study was conducted to compare different strengthening configurations used to improve shear capacity of the RC T-beams, including two-sided strengthening plates, one-sided strengthening plates, vertical strips and U-shaped strengthening along the whole length.

II. Numerical Investigation

The current study investigated numerically the shear behavior of RC T-beams strengthened with UHPFRC plates using different strengthening configurations. The non-linear finite element analysis (FEA) software ABAQUS [19] was used to develop a 2D shell element model presenting the shear behavior of UHPFRC strengthened RC T-beams.

2.1. Elements and meshing

All beams were simulated using 2D shell element model in order to reduce the central processing unit (CPU) time. In addition, in order to exploit symmetry, one half of beam was simulated in ABAQUS software. The concrete, UHPFRC, loading plates and supports were simulated using 4-node bilinear, reduced integration, hourglass control elements (CPS4). Then a 2-node linear 2D truss (T2D2) element was used to model the steel reinforcement and stirrups. An approximate mesh size 25 × 25 mm was assumed to obtain accurate results consistent with experimental results.

2.2. Modeling of materials

2.2.1. Concrete and UHPFRC

ABAQUS include three models for simulate the nonlinear behavior of concrete and UHPFRC. The existing models are the concrete damage plasticity, the concrete smeared cracking and the brittle cracking model. In the current study, the concrete damage plasticity (CDP) model is used to simulate the concrete and UHPFRC behavior.

The CDP model assumes that the uniaxial tensile and compressive response of concrete is characterized by damaged plasticity, as shown in Fig. 1. Under uniaxial tension the stress-strain response follows a linear elastic relationship until the value of the failure stress, σ_{to}, is reached. The failure stress corresponds to the onset of micro-cracking in the concrete material. Beyond the failure stress the formation of micro-cracks is represented macroscopically with a softening stress-strain response, which induces strain localization in the concrete structure. Under uniaxial compression the response is linear until the value of initial yield, σ_{co}, was reached. In the plastic regime the response is typically characterized by strain hardening followed by strain softening beyond the ultimate stress, σ_{cu}. As shown in Fig. 1, when the concrete specimen is unloaded from any point on the strain softening branch of the stress-strain curves, the unloading response is weakened: the elastic stiffness of the material appears to be damaged (or degraded). The degradation of the elastic stiffness is characterized by two damage variables, concrete tension and compression damage parameters (d_t and d_c). The values of d_t and d_c used in the current study were calculated by Equations (1) and (2) respectively according to Birtel et al [20].

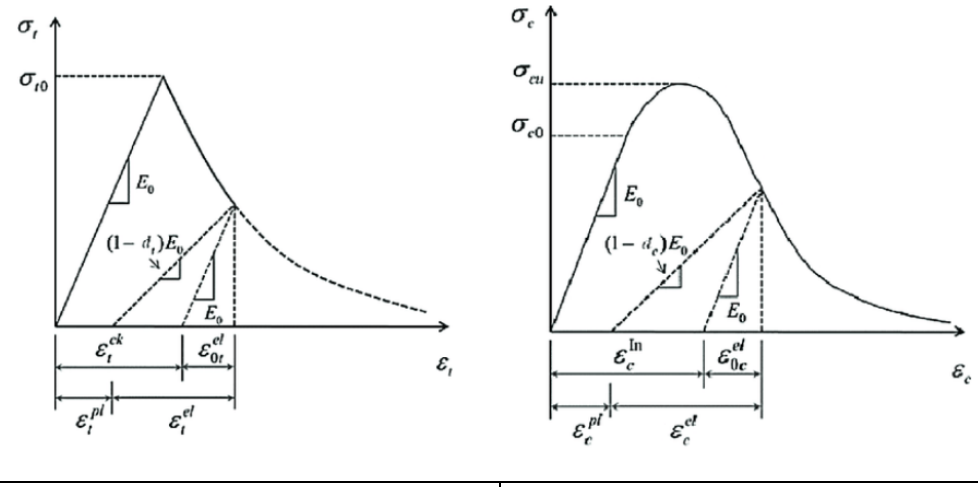

(a) Tension	(b) Compression

Fig. 1. Damage variables [19]

$$d_c = 1 - \frac{\sigma_c E_c^{-1}}{\epsilon_c^{pl}\left(\frac{1}{b_c}-1\right)+\sigma_c E_c^{-1}} \quad (1) \qquad d_t = 1 - \frac{\sigma_t E_c^{-1}}{\epsilon_t^{pl}\left(\frac{1}{b_t}-1\right)+\sigma_t E_c^{-1}} \quad (2)$$

where: d_c = Concrete compression damage parameter; σ_c = Compressive stress; E_c = concrete young's modulus; ϵ_c^{pl} = Plastic strain corresponding to compressive stress; b_c= Constant with range $0 < b_c < 1$; d_t = Concrete tension damage parameter; σ_t = Tensile stress; ϵ_t^{pl} = Plastic strain corresponding to tensile stress; b_t= Constant with range $0 < b_t < 1$.

2.2.2. Steel reinforcement

The reinforcing steel material was mostly defined by bi-linear behavior, which is represented as an elastic-perfectly plastic relationship as shown in Fig. 2. The tension and compression behaviors are identical. To

draw the stress strain curve for the reinforcing steel material, some items must be considered, such as: the yield stress (f_y), the steel young's modulus (E_s) and the ultimate strain (ε_u). The contact between reinforcing steel bar and concrete was simulated using embedded region (full bond), where, the concrete is the host.

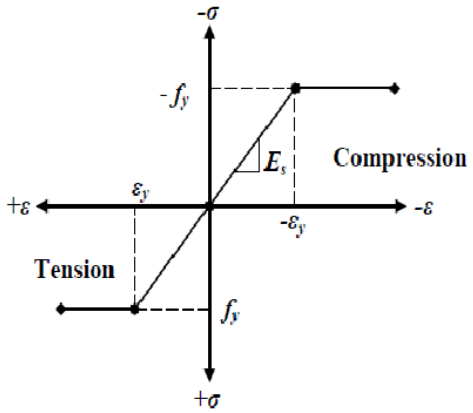

Fig. 2. Behavior of reinforcing steel bar in tension and compression

2.2.3. Contact between UHPFRC and concrete

In order to simulate the contact behavior between UHPFRC and concrete surface in 2D shell element model, connector elements with damaged and elastic-plastic behavior have been used. The behavior of contact was followed by traction-separation model in [19], the traction-separation model assumes initially linear elastic behavior followed by the initiation and evolution of damage as shown in Fig. 3. The interface thickness is considered insignificantly small, and the initial stiffness K_{ss}, K_{tt}, and K_{nn} in the two shear and the normal directions respectively calculated from Equations (3) and (4) according to Obaidat et al. [21]:

$$K_{ss} = K_{tt} = \frac{1}{\frac{t_i}{G_i}+\frac{t_c}{G_c}} \qquad (3) \qquad K_{nn} = \frac{1}{\frac{t_i}{E_i}+\frac{t_c}{E_c}} \qquad (4)$$

where: t_i = resin thickness; t_c = concrete thickness; G_i = shear modulus of resin; G_c = shear modulus of concrete; E_i = modulus of elasticity of resin; E_c = modulus of elasticity of concrete.

Damage is assumed to initiate when the maximum contact stress ratio (as defined in the expression below) reaches a value of one. This criterion can be calculated from Equation (5):

$$max\left\{\frac{\sigma_n}{\sigma_n^o}, \frac{\tau_t}{\tau_t^o}, \frac{\tau_s}{\tau_s^o}\right\} = 1 \qquad (5)$$

where: σ_n = cohesive tensile strength; σ_n^o = concrete tensile strength; τ_t and τ_s = cohesive shear stress; τ_t^o and τ_s^o = concrete shear stress = 1.5 MPa, according to [21].

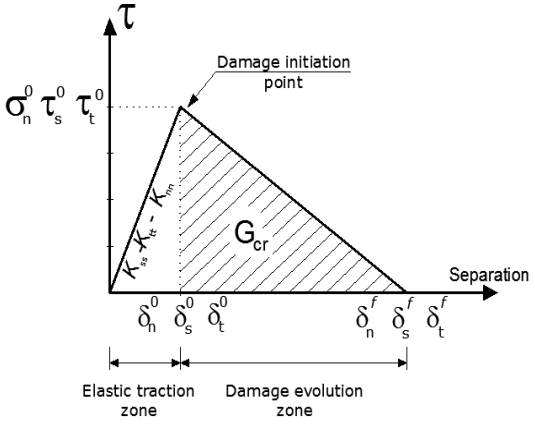

Fig. 3. Simple bilinear traction-separation law [19]

Damage evolution can be defined based on the energy that is dissipated as a result of the damage process, also called the fracture energy. The fracture energy is equal to the area under the traction-separation curve. The Benzeggagh-Kenane fracture criterion is particularly useful when the critical fracture energies during separation purely along the first and the second shear directions are the same; i.e. $G_s^C = G_t^C$. It is given by Equation (6):

$$G_n^C + (G_s^C - G_n^C)\left\{\frac{G_S}{G_T}\right\}^\eta = G^C \qquad (6)$$

where $G_S = G_s + G_t$, $G_T = G_n + G_S$ and η is the cohesive parameter. The values used in the current study were G_n^C = 90 J/m^2, $G_s^C = G_t^C$ = 900 J/m^2 and η = 1.45, according to [21].

III. Numerical Validation

In order to validate the reliability and applicability of the 2D non-linear finite element model, the results of model were compared to the experimental results available in literature [8,10,18].

Panigrahi et al. [8] studied experimentally the shear behavior of RC T-beams strengthened with externally bonded GFRP sheets. The strengthening sheets were affixed to beam surface using epoxy adhesive and tested under four-point bending. The parameters included, GFRP amount and distribution (continuous sheets versus strips), bonded surface (two sides versus U-wrap), number of GFRP layers, and U-wrap with and without end anchor. The experimental program was consisted of twelve number of RC beams with a T-shaped cross section. One of these twelve number of beams was not strengthened and was considered as a control beam (specimen CB), this beam was chosen in the current study to validate the beam numerical models. The control beam is 1300 mm length and reinforced with two 20 mm diameter and one 10 mm diameter steel rebars in tension side in order to guarantee a shear failure.

Al-Osta et al. [10] investigated experimentally and numerically the flexural behavior of RC beams of rectangular section strengthened with UHPFRC plates. Two different techniques were used to bond the strengthening plates to beam surface. The first technique was that the concrete beam surface was sandblasted to an average depth 2 mm and casting UHPFRC layer over it. The second technique was that the UHPFRC plates was bonded to the concrete beam surface using epoxy adhesive. The experimental work was consisted of four RC beams in each technique (one control beam and three strengthened beams). The RC beams before strengthening were reinforced with two 10 mm diameter steel rebars at tension and compression sides and 8 mm diameter steel rebars as shear reinforcement spaced at 50 mm centre to centre. All beams were tested under a four-point loading and strengthened with UHPFRC plates of thickness 30 mm in three different strengthening configurations in each technique; (1) bottom side strengthening; (2) two longitudinal sides strengthening; (3) three sides strengthening. Specimens RC-Control and RC-3 SJ were the control beam and the strengthened beam respectively. Moreover, these two specimens were chosen in the current study to validate the beam numerical models.

Sakr et al. [18] presented experimentally and numerically the shear behavior of RC beams of rectangular section strengthened with prefabricated UHPFRC plates and tested it under a four-point loading. In order to guarantee high quality and ease the strengthening procedure on site applications, the concrete beam surface was roughened using a steel hammer, then the UHPFRC plate was provided over it using epoxy adhesive. The control beam had dimensions 150 mm width, 300 mm depth and 2000 mm total length. This beam reinforced with two 18 mm and two 10 mm diameter steel rebars at tension and compression sides, respectively in addition to 8 mm diameter steel rebar as shear reinforcement. The specimens C-S and ST-1S were the control beam and the strengthened beams, respectively, these specimens were chosen in the current study to validate the beam numerical models.

Fig. 4 shows the cross section and reinforcement details of considered literature experimental studies. Additionally, the material properties of concrete, UHFRPC and steel are shown in Table 1.

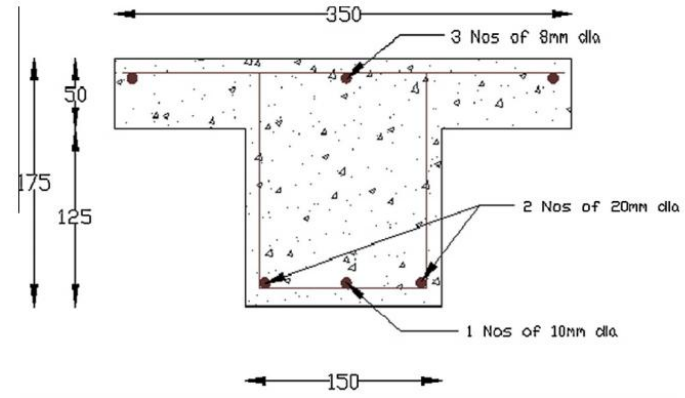

(a) Specimen CB [8]

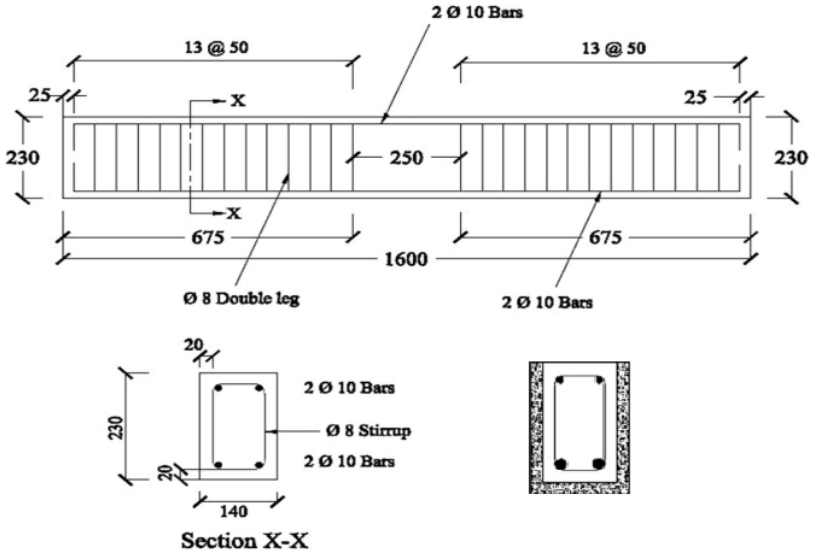

(b) Specimens RC-Control and RC-3 SJ [10]

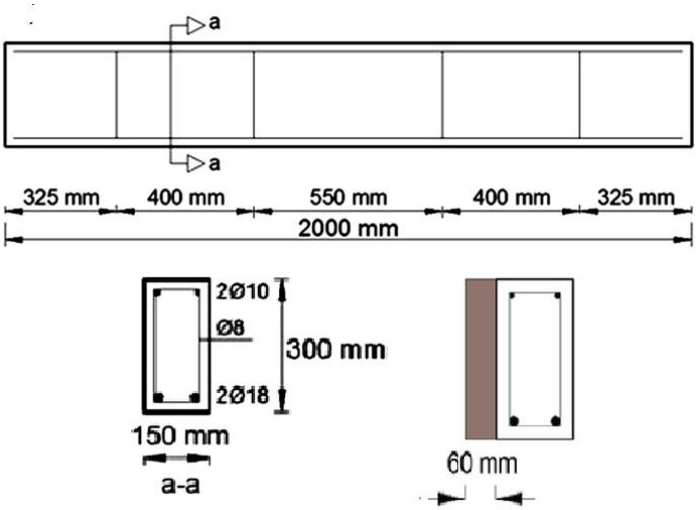

(c) Specimens C-S and ST-1S [18]

Fig. 4. Cross section and reinforcement details of specimens used in validation

Table 1: Material properties of literature studies that used in validation

Literature study	*Compressive strength f_c (MPa)*		*Tensile strength f_t (MPa)*		*Steel rebars f_y (MPa)*	
	Concrete	*UHPFRC*	*Concrete*	*UHPFRC*		
					Φ (mm)	f_y
Panigrahi et al. [8]	22.21	-------	2.8	-------	8	523
					10	529
					20	470
Al-Osta et al. [10]	54	128	4.5	7	610	
					Φ (mm)	f_y
Sakr et al. [18]	30	135.37	2.5	11.50	8	406
					10	559
					18	478

For all validated specimens, the modulus of elasticity and Poisson's ratio of concrete, UHPFRC and steel rebars are shown in Table 2. The nonlinear behavior of concrete and UHPFRC of all specimens that used in validation shown in Fig. 5. Additionally, the concrete damage plasticity model (CDPM) parameters of concrete and UHPFRC are shown in Table 3. Moreover, the number of elements and number of degrees of freedom for all validated specimens are listed in Table 4.

Table 2: Modulus of elasticity and Poisson's ratio of all validated specimens

Literature study	*Modulus of elasticity (MPa)*			*Poisson's ratio*		
	Concrete	*UHPFRC*	*Steel rebars*	*Concrete*	*UHPFRC*	*Steel rebars*
Panigrahi et al. [8]	20700	-------	200000	0.2	-------	0.3
Al-Osta et al. [10]	34000	46000	200000	0.15	0.15	0.3
Sakr et al. [18]	24000	47000	200000	0.2	0.22	0.3

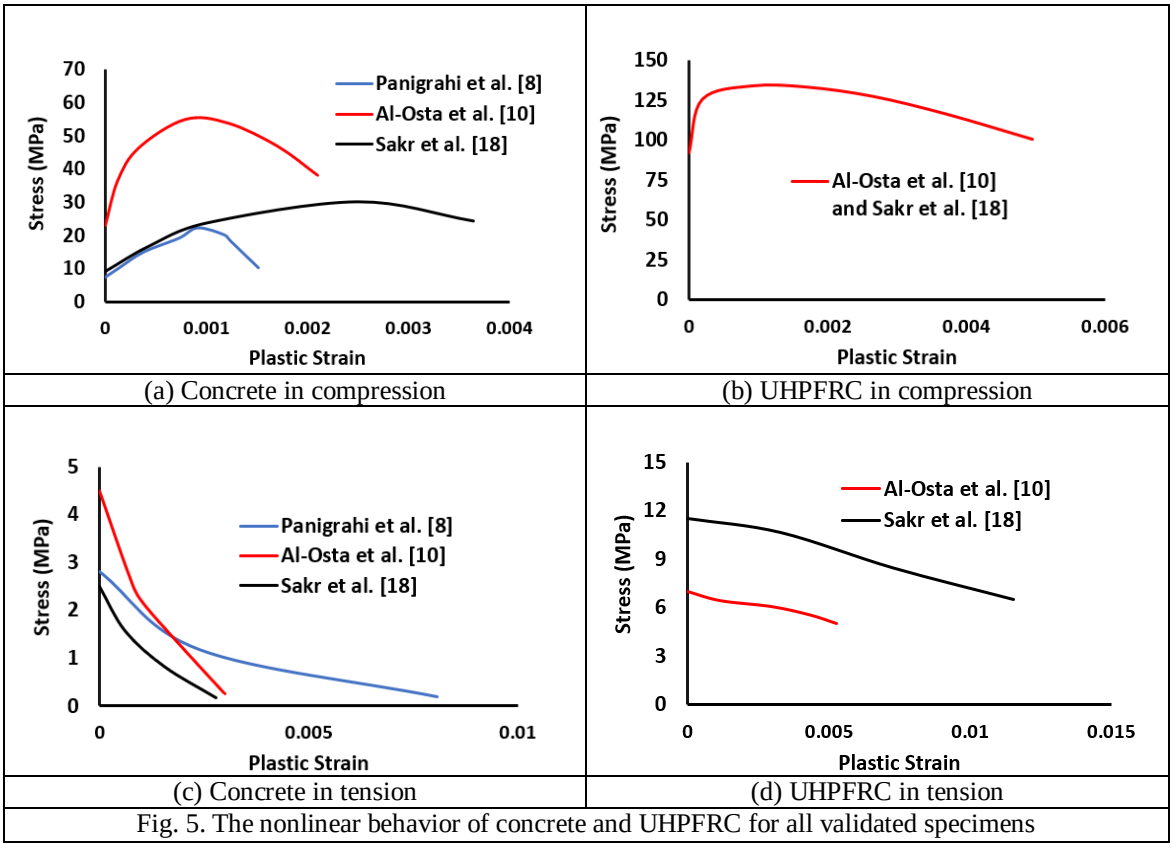

(a) Concrete in compression

(b) UHPFRC in compression

(c) Concrete in tension

(d) UHPFRC in tension

Fig. 5. The nonlinear behavior of concrete and UHPFRC for all validated specimens

Table 3: Damage parameters for UHPFRC and concrete

Literature study	*Material*	*Dilation angle**	*Eccentricity**	f_{bo}/f_{co}*	*K**	*Viscosity parameter*
Panigrahi et al. [8]	Concrete	38	0.1	1.16	0.667	0
Al-Osta et al. [10]	Concrete	36				
	UHPFRC	36				
Sakr et al. [18]	Concrete	15				
	UHPFRC	36				

*Dilation angle: the inclination of the plastic flow potential in high confining pressures, the value of dilation angle is equal to the friction angle in low stresses and this value decreased in higher level of confinement stress and plastic strain. Maximum value of it 56.3° and minimum value close to 0°.
*Eccentricity: the flow potential eccentricity.
*f_{bo}/f_{co}: the proportion of initial equibiaxial compressive yield stress and initial uniaxial compressive yield stress.
*K: the ratio of the second stress invariant in the tensile meridian to compressive meridian for any defined value of the pressure invariant at initial yield.

Table 4: Model size for all validated specimens

Literature study	*Specimens*	*Number of shell element*	*Number of truss element*	*Total number of elements*	*Number of degrees of freedom (DOF)*
Panigrahi et al. [8]	CB	182	60	242	648
Al-Osta et al. [10]	RC-Control	292	172	464	1008
	RC-3 SJ	612	172	784	2097
Sakr et al. [18]	C-S	976	98	1074	3219
	ST-1S	1936	98	2034	6378

3.1. Load-deflection responses

The load-deflection curves for all validated specimens are shown in Fig. 6 and compared with the results of literature experimental studies. The finite element analysis shows acceptable results and close to the literature experimental results.

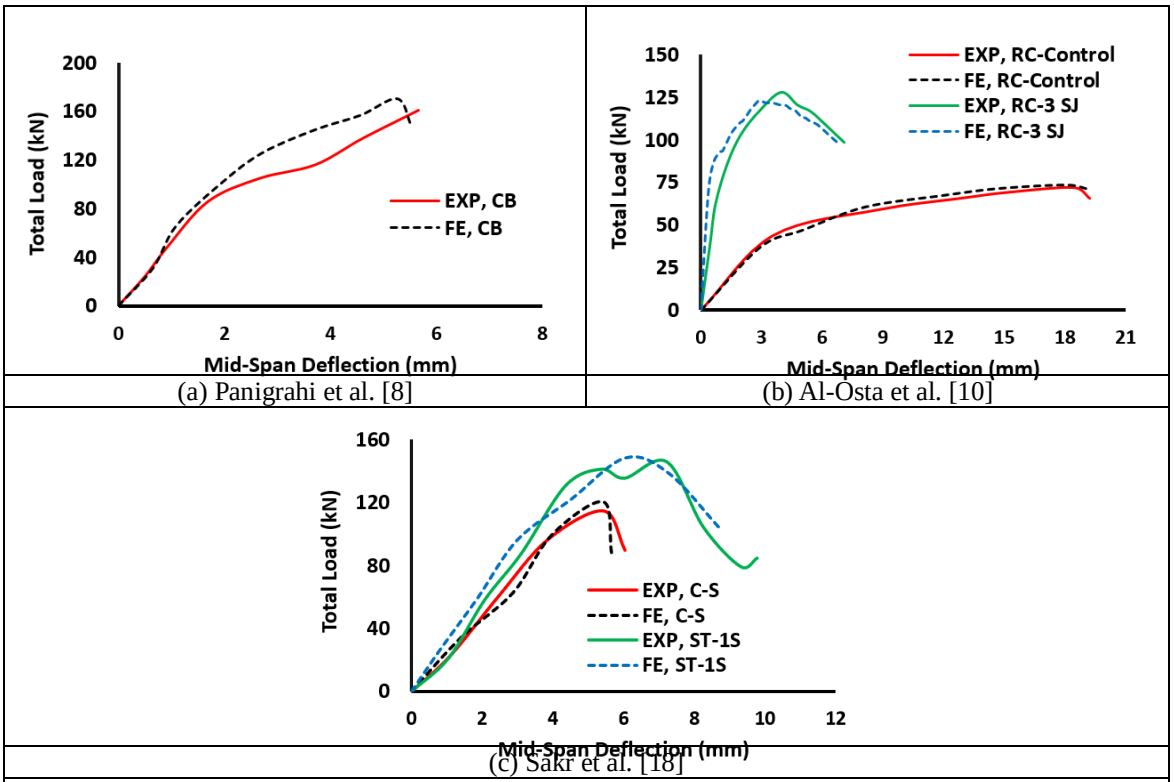

(a) Panigrahi et al. [8]

(b) Al-Osta et al. [10]

(c) Sakr et al. [18]

Fig. 6. Experimental versus numerical load- deflection curves for all validated specimens

3.2. Failure mechanism

The numerical investigation presented failure patterns identical to the failure patterns resulting from the experimental works. Unfortunately, the specimen CB with the T-section shape collapsed in shear, in addition to the specimen C-S, also collapsed in the shear. The specimen ST-1S collapsed in shear in addition to partial separation of the strengthening plate at the lower part. The specimens RC-Control and RC-3 SJ were collapsed ductile flexurally. Figures 7-9 shows a comparison between experimental and numerical failure patterns for some specimens that used for verification.

(a) Experimental

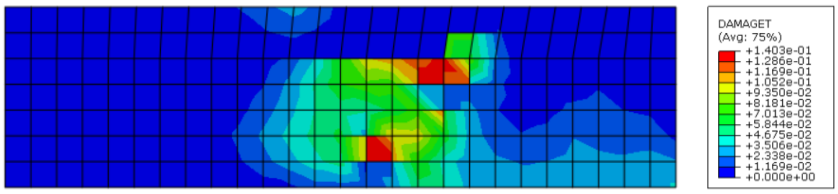

(b) Numerical

Fig. 7. Experimental versus numerical failure pattern of specimen CB

(a) Experimental

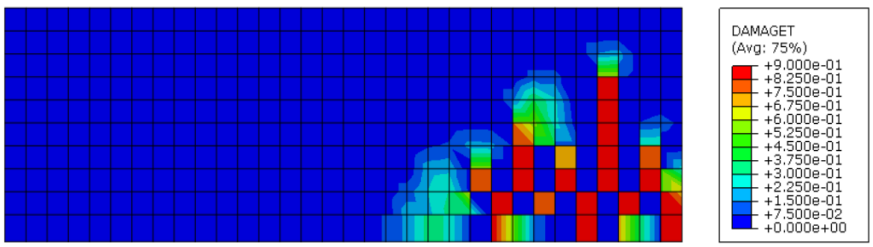

(b) Numerical

Fig. 8. Experimental versus numerical failure pattern of specimen RC-3 SJ

(a) Experimental

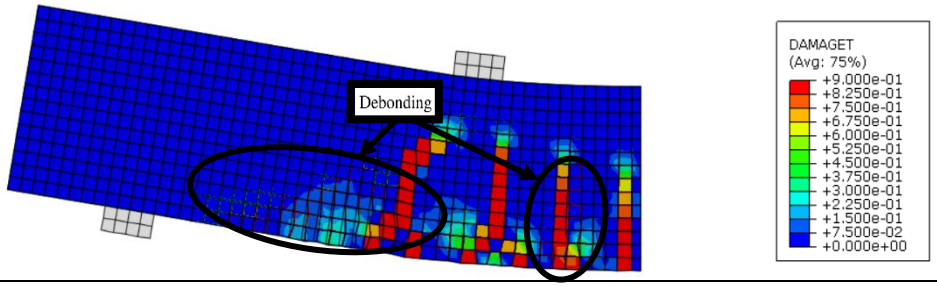

(b) Numerical

Fig. 9. Experimental versus numerical failure pattern of specimen ST-1S

IV. Parametric Study

The 2D shell element model was used to make the numerical investigation and one half of beam is modelled to take the advantage of symmetry. The parametric study investigated based on the properties of concrete, UHPFRC, reinforcement and boundary conditions that used in validation of specimen RC-3 SJ. The control beam specimen (CB-S) shown in Fig. 10 of T-section shape was used in the current study to be the non-strengthened beam. This beam is overdesigned in flexure as per ACI-318 [22] to guarantee a shear failure. Based on design, two 25 mm and two 12 mm diameter steel rebars were used at tension and compression side in addition to 8 mm diameter stirrups as a shear reinforcement and the slab thickness and width were assumed to be 75 mm and 500 mm respectively with reinforcement of three 8 mm diameter steel rebars.

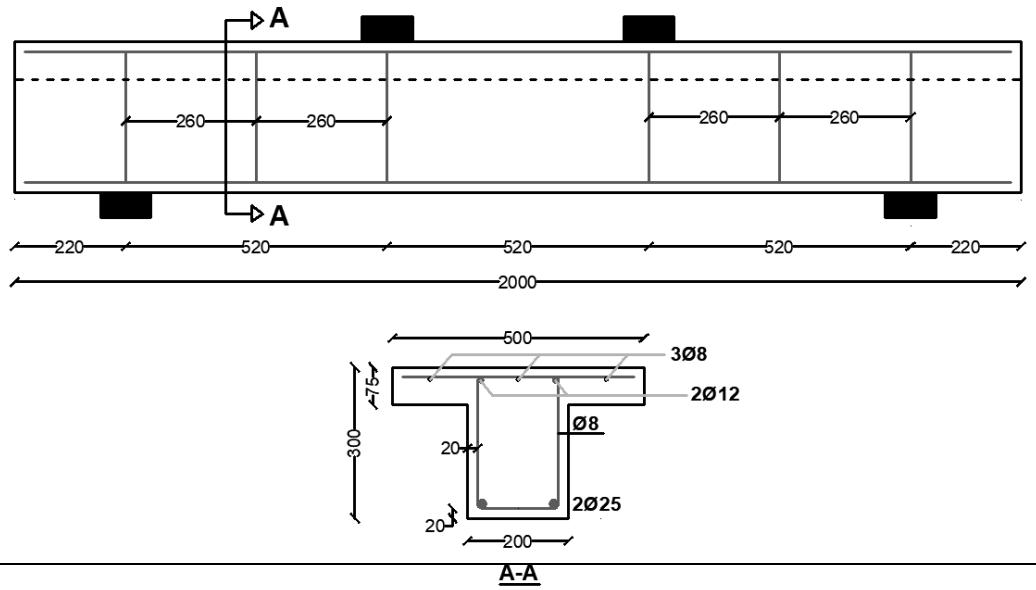

Fig. 10. Cross section and reinforcement details of control specimen (CB-S)

The results of specimen CB-S which obtained using ABAQUS software showed that this beam collapsed in shear and this agreed well with the pre-design. The load-deflection response is shown in Fig. 11 in addition to the failure pattern and plastic strain distribution of reinforcement of this specimen are shown in Fig. 12. Different strengthening techniques were used to improve the shear capacity of specimen CB-S in an attempt to change the failure pattern from shear to ductile flexural. These techniques included two-sided strengthening plates, one-sided strengthening plates, vertical strips and U-shaped strengthening technique. All strengthening techniques used were made using UHPFRC plates along the whole length of specimen CB-S except the technique of vertical strips was consisted of separated strips of UHPFRC distributed at equal distances from the length of the beam.

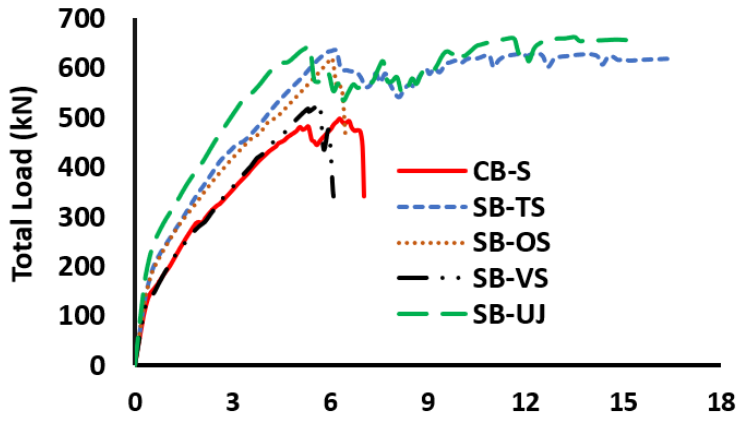

Fig. 11. Load-deflection response

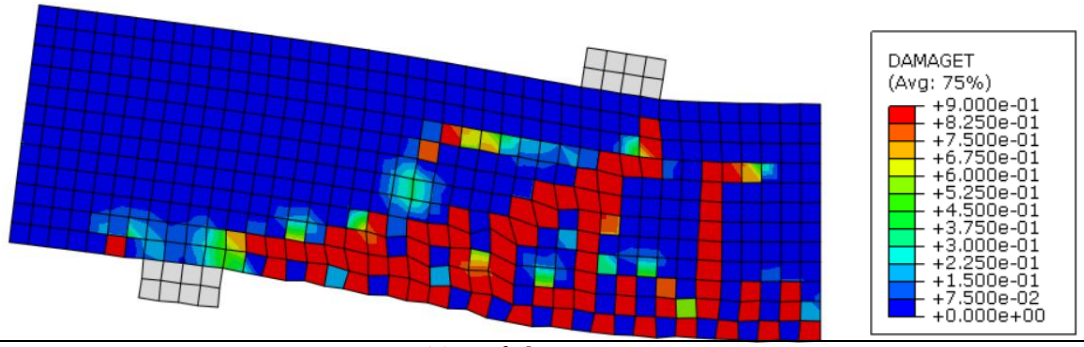

(a) 2D failure pattern

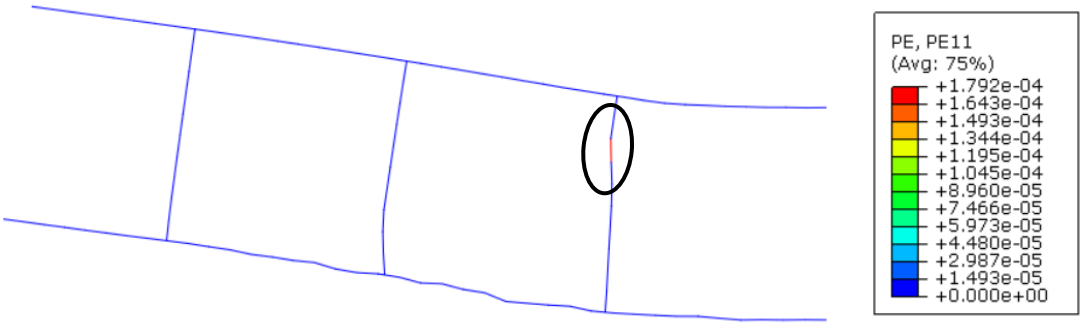

(b) Plastic strain distribution of reinforcement

Fig. 12. FEA results of specimen CB-S

4.1. Two-sided strengthening technique

Strengthening of 30 mm thickness UHPFRC plates was used on both sides of the RC T-beam along its entire length, as shown in Fig. 13. The numerical study showed the clear effect of the strengthening on both sides, as it was found from the load-deflection curve shown in Fig. 11 that the strengthened specimen SB-TS from both sides led to a noticeable increase in the ultimate maximum load by 27.4% compared to the control beam specimen CB-S, as well as an increase in the stiffness and ductility. Through the collapse pattern shown in Fig. 14a, it was found that the specimen SB-TS was able to transform the collapse pattern in the control beam from shear failure to ductile flexural failure. It was also noted that there was a separation of the strengthening plate (debonding) from the concrete body in the lower part of the beam as well as in the upper part directly below the RC slab. Fig. 14b shows the plastic strain distribution of reinforcement of specimen SB-TS.

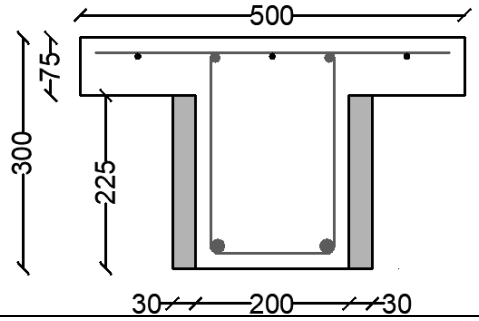

Fig. 13. Strengthening using two-sided UHPFRC plates

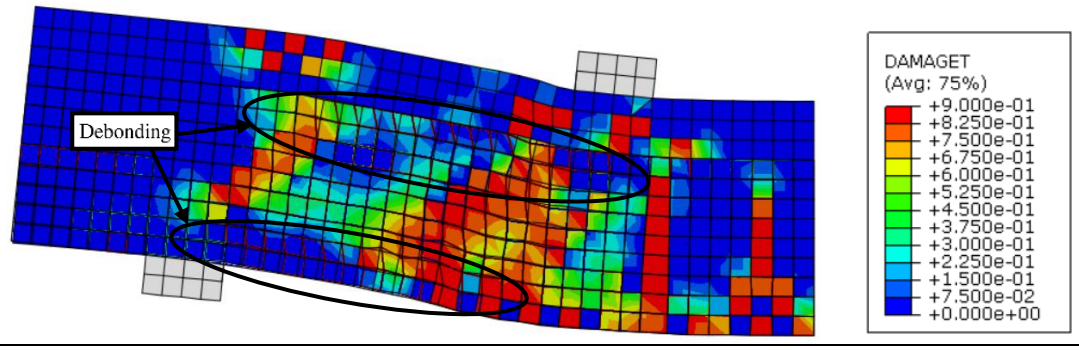

(a) 2D failure pattern

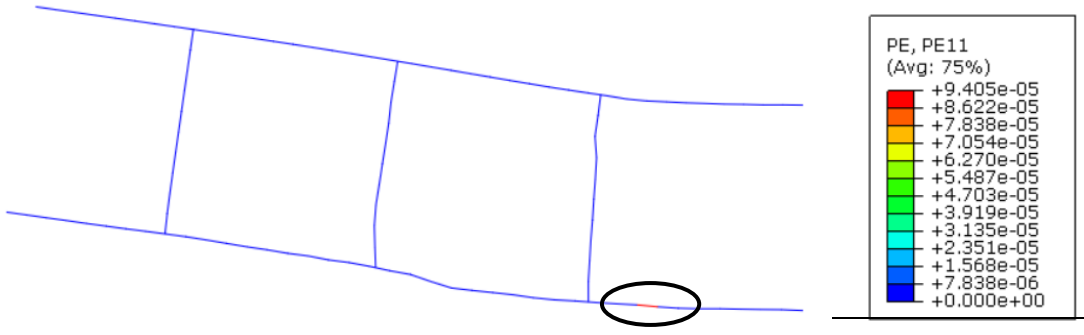

(b) Plastic strain distribution of reinforcement

Fig. 14. FEA results of specimen SB-TS

4.2. One-sided strengthening technique

Two-sided strengthening of the RC T-beams may not be accessible in some cases. Therefore, the situation requires only one-sided strengthening. So, in this part one-sided strengthening was used along the entire length of RC T-beam and the strengthening plate thickness in this case was chosen to be the sum of strengthening plates thickness used in the case of two-sided strengthening as shown in Fig. 15. Through the load deflection curve shown in Fig. 11, it was found that the one-sided strengthening (specimen SB-OS) gives a noticeable increase in the ultimate maximum load and stiffness compared to the control beam without any

improvement in ductility. The value of the increase in the ultimate maximum load was 24.16% and this increase is very close to the case of the strengthening from both sides, but the difference between the two cases is that the one-sided specimen SB-OS was able to increase the value of the load, but it was not able to change the collapse pattern of the control beam, so the failure is still a shear failure with a fully noticeable debonding of strengthening plates in the shear span zone as shown in Fig. 16a. Additionally, the plastic strain distribution of reinforcement of specimen SB-OS is shown in Fig. 16b.

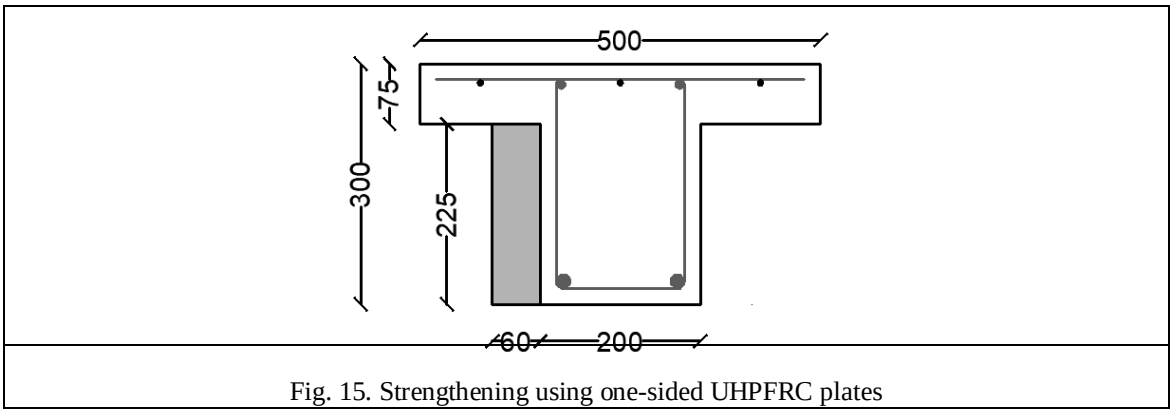

Fig. 15. Strengthening using one-sided UHPFRC plates

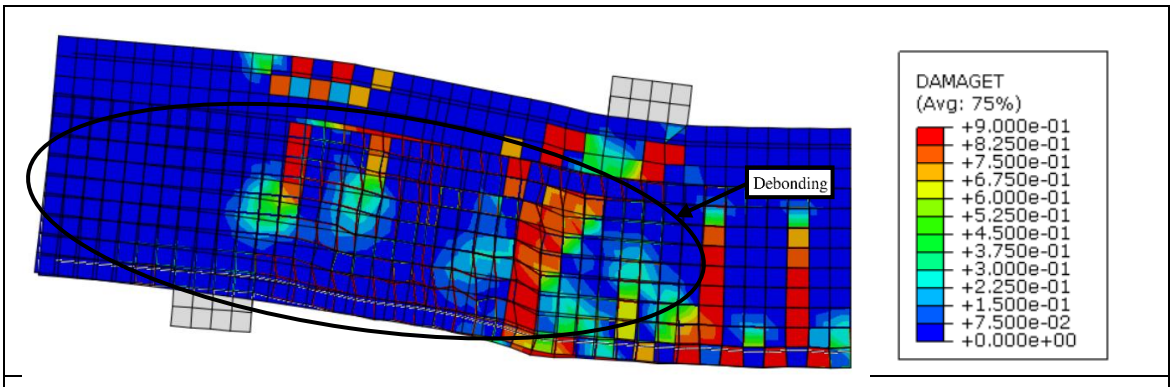

(a) 2D failure pattern

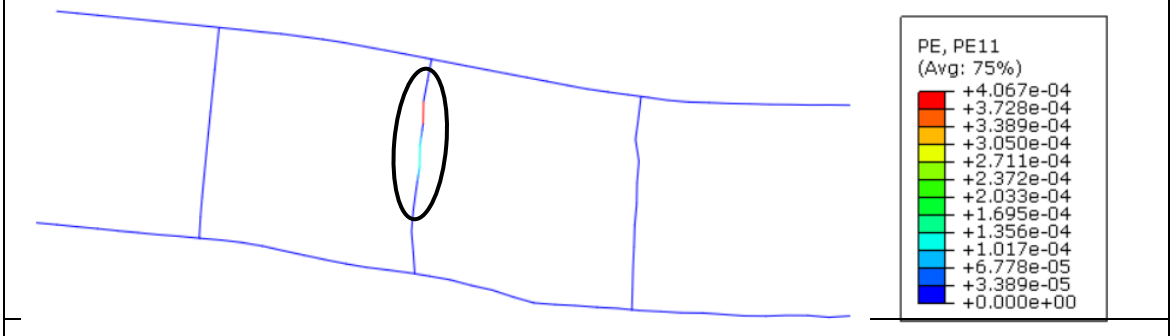

(b) Plastic strain distribution of reinforcement

Fig. 16. FEA results of specimen SB-OS

4.3 Vertical strips strengthening technique

Mofidi et al. [23] investigated experimentally the shear behavior of RC T-beams strengthened with externally bonded CFRP vertical strips and sheets. The strip width to strip spacing ratio was one of the studied parameters in addition to the effect of CFRP-strips location with respect to steel-stirrups location. On the one hand, CFRP strips placed in the same locations of steel stirrups. On the other hand, CFRP strips placed midway between steel-stirrup locations. The results of changing the strip width to strip spacing ratio showed that the contribution of CFRP to shear in beams strengthened by strips distributed at wider distances was greater than those strengthened by strips distributed at narrower distances. Installing CFRP strips midway between steel-stirrup locations achieved ultimate maximum load greater than installing these strips at the same locations of

steel stirrups.

In this part, vertical strips of UHPFRC affixed on both sides of RC T-beam was used. Each strip had dimensions of 100 mm width, 30 mm thickness and distributed at distances 292 mm center to center as shown in Fig. 17. According to the load-deflection curve shown in Fig. 11, it was found that the strengthened specimen SB-VS with vertical strips was the least of strengthened beams in terms of increase the ultimate maximum load compared to the control beam, this increase was 5.98% greater than the control beam. There is no difference was observed in stiffness or ductility of specimen SB-VS compared to the control beam. The specimen SB-VS was not able to change the failure pattern of control beam, the failure still a shear failure in addition to partial debonding as shown in Fig. 18.

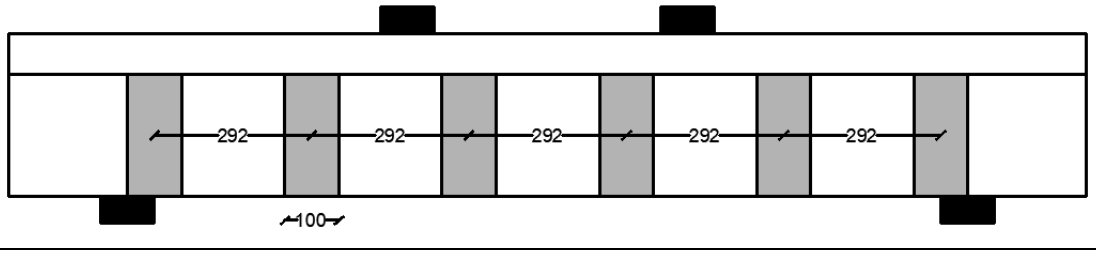

Fig. 17. Strengthening using separated vertical strips of UHPFRC

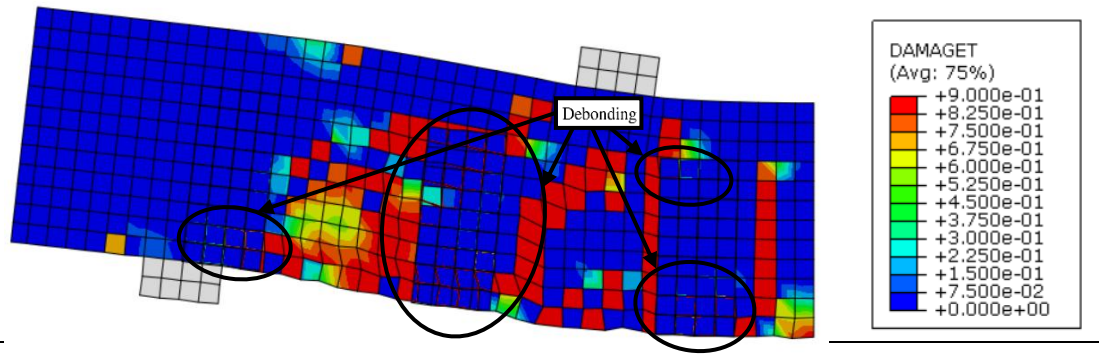

Fig. 18. 2D failure mechanism of specimen SB-VS

4.4 U-shaped strengthening technique

The purpose of U-shaped strengthening is to resist both shear and flexure. The vertical sides resist shear, while the lower side resist flexure. Therefore, it was expected to obtain the maximum load from this case of strengthening compared to other cases. The two vertical plates and bottom plate had a thickness of 30 mm as shown in Fig. 19. Through the load-deflection curve shown in Fig. 11, it was found that the specimen SB-UJ increased the ultimate maximum load by 32.91% compared to the control beam. As expected, this is the maximum increase of all strengthening cases that were studied. The specimen SB-UJ was able to transform the collapse pattern from shear in the control beam to a flexural failure with a clear improvement in the stiffness and ductility over all previous strengthening cases. In addition, a debonding was observed in the strengthening plate in the shear span zone as shown in the Fig. 20a. The plastic strain distribution of reinforcement of this specimen is shown in Fig. 20b. Table 5 shows a summary of results of all strengthening techniques were used.

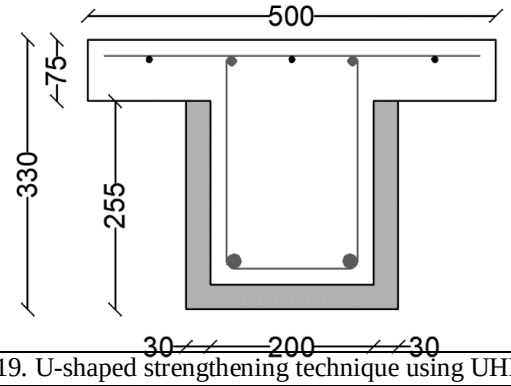

Fig. 19. U-shaped strengthening technique using UHPFRC

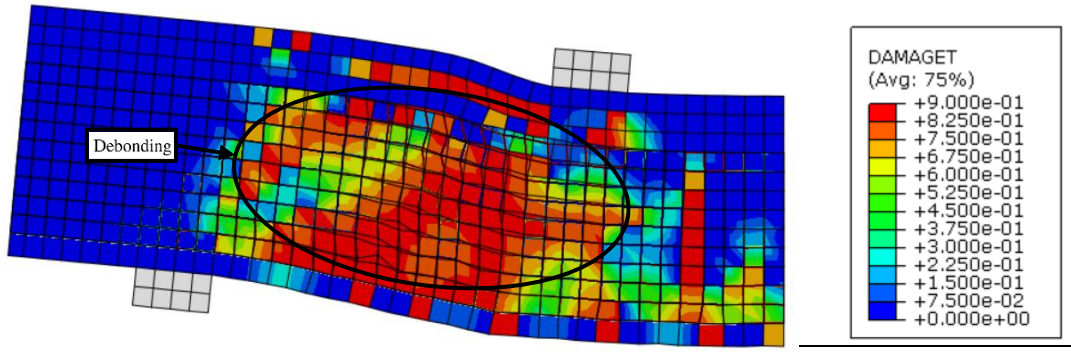

(a) 2D failure pattern

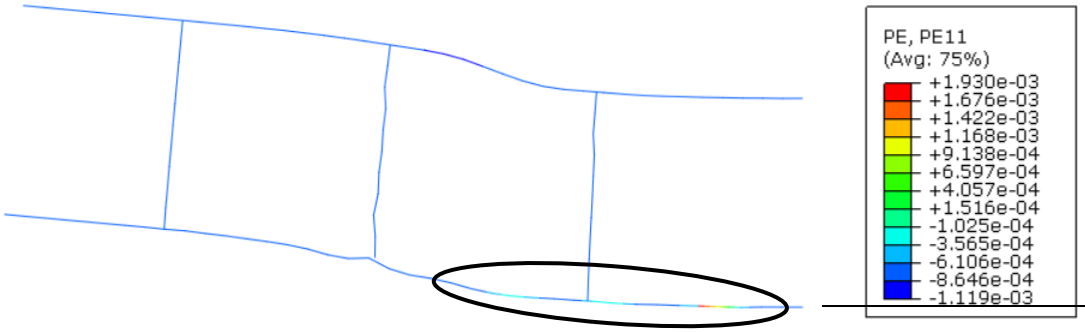

(b) Plastic strain distribution of reinforcement

Fig. 20. FEA results of specimen SB-UJ

Table 5: Summary of results of all used strengthening techniques

Specimen	*Ultimate load (kN)*	*Yield Load (kN)*	*Ultimate displacement (mm)*	*Yield displacement (mm)*	*% Increasing in load refer to control beam*
CB-S	497.906	398.298	6.3048	3.8051	----------
SB-TS	634.351	622.122	6.1828	5.7139	27.40
SB-OS	618.206	516.026	6.0507	4.5803	24.16
SB-VS	527.716	461.346	5.6871	4.4734	5.98
SB-UJ	661.788	554.811	13.522	8.3521	32.91

V. Conclusions

This paper has discussed numerically different strengthening techniques using UHPFRC plates to improve the shear resisting capacity of RC T-beams. The strengthening techniques were included, two-sided strengthening, one-sided strengthening, vertical strips, and U-shaped strengthening technique. On the base of results discussed in the paper, the following remarks can be drawn:

- 2D shell element model was able to simulate the shear behavior of RC T-beams strengthened with UHPFRC plates.

- The application of two-sided UHPFRC plates on a RC T-beam provides a noticeable increase of the ultimate maximum load, stiffness, ductility, and transfer of the collapse pattern from shear to flexural. The specimen SB-TS increased the ultimate load by 27.4% compared to the control beam.
- One-sided strengthening of RC T-beam with UHPFRC plate was able to increase the ultimate maximum load to a value close to that of two-sided strengthening but it could not change the failure pattern, so it is still shear failure. The specimen SB-1S increased the ultimate load by 24.16% compared to the control beam.
- Strengthening the RC T-beam using vertical strips of UHPFRC provided a little increase in ultimate load with no improvement in stiffness and ductility as specimen SB-VS.
- U-shaped strengthening technique was the best type of strengthening, as it gave the maximum load compared to other strengthening cases in addition to a better increase in stiffness and ductility. The specimen SB-UJ failed in flexural at 661 kN versus 497 kN of control beam specimen, which failed in shear.

References

[1]. Kang, S. T., Lee, Y., Park, Y. D., & Kim, J. K. (2010). Tensile fracture properties of an Ultra High Performance Fiber Reinforced Concrete (UHPFRC) with steel fiber. Composite structures, 92(1), 61-71.

[2]. Habel, K., Viviani, M., Denarié, E., & Brühwiler, E. (2006). Development of the mechanical properties of an ultra-high performance fiber reinforced concrete (UHPFRC). Cement and Concrete Research, 36(7), 1362-1370.

[3]. Benson, S. D. P., & Karihaloo, B. L. (2005). CARDIFRC®–Development and mechanical properties. Part III: Uniaxial tensile response and other mechanical properties. Magazine of Concrete Research, 57(8), 433-443.

[4]. Xu, M., & Wille, K. (2015). Fracture energy of UHP-FRC under direct tensile loading applied at low strain rates. Composites Part B: Engineering, 80, 116-125.

[5]. Yoo, D. Y., Shin, H. O., Yang, J. M., & Yoon, Y. S. (2014). Material and bond properties of ultra high performance fiber reinforced concrete with micro steel fibers. Composites Part B: Engineering, 58, 122-133.

[6]. Lampropoulos, A. P., Paschalis, S. A., Tsioulou, O. T., & Dritsos, S. E. (2016). Strengthening of reinforced concrete beams using ultra high performance fibre reinforced concrete (UHPFRC). Engineering Structures, 106, 370-384.

[7]. Habel, K., Denarié, E., & Brühwiler, E. (2006). Structural response of elements combining ultrahigh-performance fiber-reinforced concretes and reinforced concrete. Journal of structural engineering, 132(11), 1793-1800.

[8]. Panigrahi, A. K., Biswal, K. C., & Barik, M. R. (2014). Strengthening of shear deficient RC T-beams with externally bonded GFRP sheets. Construction and Building Materials, 57, 81-91.

[9]. Zhang, Y., Li, X., Zhu, Y., & Shao, X. (2020). Experimental study on flexural behavior of damaged reinforced concrete (RC) beam strengthened by toughness-improved ultra-high performance concrete (UHPC) layer. Composites Part B: Engineering, 186, 107834.

[10]. Al-Osta, M. A., Isa, M. N., Baluch, M. H., & Rahman, M. K. (2017). Flexural behavior of reinforced concrete beams strengthened with ultra-high performance fiber reinforced concrete. Construction and Building Materials, 134, 279-296.

[11]. Bahraq, A. A., Al-Osta, M. A., Ahmad, S., Al-Zahrani, M. M., Al-Dulaijan, S. O., & Rahman, M. K. (2019). Experimental and numerical investigation of shear behavior of RC beams strengthened by ultra-high performance concrete. International Journal of Concrete Structures and Materials, 13(1), 1-19.

[12]. Tayeh, B. A., Bakar, B. A., Johari, M. M., & Voo, Y. L. (2013). Utilization of ultra-high performance fibre concrete (UHPFC) for rehabilitation–a review. Procedia Engineering, 54, 525-538.

[13]. Tayeh, B. A., Naja, M. A., Shihada, S., & Arafa, M. (2019). Repairing and strengthening of damaged RC columns using thin concrete jacketing. Advances in Civil Engineering, 2019.

[14]. Tayeh, B. A., Bakar, B. A., Johari, M. M., & Voo, Y. L. (2013). Evaluation of bond strength between normal concrete substrate and ultra high performance fiber concrete as a repair material. Procedia Engineering, 54, 554-563.

[15]. Tayeh, B. A., Bakar, B. A., & Johari, M. M. (2013). Characterization of the interfacial bond between old concrete substrate and ultra high performance fiber concrete repair composite. Materials and structures, 46(5), 743-753.

[16]. Tayeh, B. A., Bakar, B. A., Johari, M. M., & Ratnam, M. M. (2013). The relationship between substrate roughness parameters and bond strength of ultra high-performance fiber concrete. Journal of Adhesion Science and Technology, 27(16), 1790-1810.

[17]. Tayeh, B. A., Bakar, B. A., Johari, M. M., & Voo, Y. L. (2012). Mechanical and permeability properties of the interface between normal concrete substrate and ultra high performance fiber concrete overlay. Construction and building materials, 36, 538-548.

[18]. Sakr, M. A., Sleemah, A. A., Khalifa, T. M., & Mansour, W. N. (2019). Shear strengthening of reinforced concrete beams using prefabricated ultra-high performance fiber reinforced concrete plates: Experimental and numerical investigation. Structural Concrete, 20(3), 1137-1153.

[19]. ABAQUS Theory Manual (6.14) (2014). Dassault Systemes, Providence, RI, USA.

[20]. Birtel, V., & Mark, P. (2006, May). Parameterised finite element modelling of RC beam shear failure. In ABAQUS users' conference (Vol. 14).

[21]. Obaidat, Y. T., Heyden, S., & Dahlblom, O. (2010). The effect of CFRP and CFRP/concrete interface models when modelling retrofitted RC beams with FEM. Composite Structures, 92(6), 1391-1398.

[22]. ACI-Committee 318 (ACI 318-08), "Building code requirement for structural concrete and commentary"", American Concrete Institute.

[23]. Mofidi, A., & Chaallal, O. (2011). Shear strengthening of RC beams with externally bonded FRP composites: Effect of strip-width-to-strip-spacing ratio. Journal of Composites for Construction, 15(5), 732-742.